C. R. Physique 15 (2014) 300–308

Contents lists available at ScienceDirect

Comptes Rendus Physique

www.sciencedirect.com

Ultra-high-energy cosmic rays / Rayons cosmiques de ultra-haute énergie

Cosmic rays from the knee to the ankle

Rayons cosmiques du genou à la cheville

Mario Edoardo Bertaina *

Department of Physics, University of Torino, Via Pietro Giuria, 1, 10125 Torino, Italy

ARTICLE INFO

Article history:
Available online 19 March 2014

Keywords:
Cosmic rays
Energy spectrum
Mass composition
Anisotropy
Knee
Ankle

Mots-clés :
Rayons cosmiques
Spectre en énergie
Composition en masse
Anisotropies
Genou
Cheville

ABSTRACT

The shape and composition of the primary spectrum as well as the large-scale anisotropy in the arrival direction of cosmic rays are key elements to understand the origin, acceleration and propagation of the Galactic radiation. Besides the well-known knee and ankle features, the measured energy spectrum exhibits also a less pronounced but still clear deviation from a single power law between the knee and the ankle, with a spectral hardening at $\sim 2 \times 10^{16}$ eV and a steepening at $\sim 10^{17}$ eV. The average mass composition gets heavier after the knee till $\sim 10^{17}$ eV, where a bending of the heavy component is observed. An indication of a hardening of the light component just above 10^{17} eV has been measured as well. First indications of anisotropy of the arrival direction in the southern hemisphere have been reported at $\sim 10^{15}$ eV.

RÉSUMÉ

La forme et la composition du spectre des primaires ainsi que les anisotropies à grande échelle dans la distribution d'arrivée des rayons cosmiques sont des éléments clés pour comprendre l'origine, l'accélération et la propagation du rayonnement galactique. En dehors des particularités spectrales bien connues que sont le genou et la cheville, la mesure du spectre en énergie révèle également, entre ces deux particularités, une déviation claire, bien que moins prononcée, par rapport à une loi de puissance unique : le spectre se durcit jusqu'à $\sim 2 \times 10^{16}$ eV et tombe ensuite à partir de $\sim 10^{17}$ eV. La composition en masse, quant à elle, devient plus lourde après le genou, et ce jusqu'à $\sim 10^{17}$ eV, valeur à partir de laquelle elle chute rapidement. Un durcissement de la composante légère au-dessus de 10^{17} eV a aussi été mesuré. De premières indications d'anisotropies dans les mesures des directions d'arrivée depuis l'hémisphère sud ont été rapportées à $\sim 10^{15}$ eV.

* Tel.: +39 0116707492; fax: +39 0116707497.
E-mail address: bertaina@to.infn.it.

http://dx.doi.org/10.1016/j.crhy.2014.03.001
1631-0705/

1. Introduction

The paradigm of the origin of Galactic cosmic rays (CR) are supernovae, as their shock waves can provide the required power to explain the intensity of the CR radiation at least up to 10^{15} eV. This paradigm has been recently confirmed by the observations of AGILE [1] and FERMI satellites [2]. A continuous and steady source distribution in space and time would generate an energy spectrum with a simple power law for all elements. However, in a more realistic approach, sources are discrete and a possible non-uniform distribution in space and time could generate structures and changes in the spectral indexes of the primaries at certain energies. Moreover, different populations of sources could be responsible for the Galactic radiation at lower energies and extragalactic at the highest ones [3,4]. Those sources would be subject to a rigidity cutoff in the maximum energy at which the various elements are accelerated, as proposed originally by Peters [5]. Proton will cutoff first, followed by helium, carbon, silicon, iron, etc. according to:

$$E_{\max}(Z) = Z \times E_{\max}(Z = 1) \tag{1}$$

In this approach, the knee at $\sim 4 \times 10^{15}$ eV would represent the end of the spectrum of CR accelerated by supernova remnants in the Milky Way and the ankle at $\sim 4 \times 10^{18}$ eV the transition to particles from extragalactic sources. The ankle structure could be explained also in a completely different way, such as a consequence of the physical process of pair production by protons during propagation through the cosmic microwave background radiation, as proposed by Berezinsky et al. [6]. In this case, the Galactic–extragalactic transition occurs below 10^{18} eV.

A refined study of the CR primary spectrum and composition is, therefore, extremely important to address the above questions. As acceleration and propagation mechanisms in magnetic fields would lead to the same rigidity dependence, the study of large scale anisotropies in the arrival direction could provide relevant information to distinguish source and propagation effects.

The direct study of CRs by means of satellite or balloon-borne detectors is performed only at energies below 10^{15} eV (see [7] for a recent review of the subject). Close to the knee, the flux becomes of the order of 1 particle $\mathrm{m}^{-2}\,\mathrm{sr}^{-1}\,\mathrm{yr}^{-1}$. This fact prevents the possibility of a direct observation of its structure by currently planned satellite or balloon experiments. Indeed, at least hundred of events above the knee are necessary to determine its existence with enough significance.

Around the knee and at higher energies, CRs are studied by means of large arrays located at ground that measure the secondary particles produced by the primary CR cascading in the atmosphere, the so-called Extensive Air Showers (EAS). Typically, the energy is proportional to the total number of secondaries sampled at ground, while the composition is inferred either through a multi-component measurement, such as the electromagnetic and muonic components, or through the measurement of the emitted light (Cherenkov or fluorescence lights) along the longitudinal development of the shower. Despite the fact that shower arrays allow one to collect high statistics, the interpretation of the results is based on the comparison with expectations from simulation describing the EAS development in atmosphere, which are at some level inaccurate. This introduces a systematic uncertainty on the results, especially on the mass composition.

Interestingly, the TeV region allows some partial overlap between direct and indirect measurements. Several techniques have been employed recently on ground detectors that are sensitive to specific components of the CR radiation to overcome those uncertainties (for a review, see [8]). Among them, it is worth mentioning the measurement of the light component (p alone, or p+He) using hadron calorimeters [9,10], or Cherenkov light measurements in coincidence with TeV muons [11], and RPC counters at high altitude [12]. Those results are in quite good agreement with measurements by CREAM [13] balloon. In particular, the ARGO results allow one to cross-check the fluxes on an extended energy range (5–250 TeV). These results show that, when indirect measurements have the opportunity of selecting almost pure beams, their findings are in reasonable agreement with direct ones and confirm a fair representation of the EAS development in the atmosphere by simulation codes such as CORSIKA [14].

2. The knee region

The all-particle CR energy spectrum shows a distinct feature at $\sim 4 \times 10^{15}$ eV, where the power index suddenly changes from $\gamma \sim -2.7$ to $\gamma \sim -3.1$. This is the so-called 'knee' of the CR spectrum. Since its discovery in 1958 by Kulikov and Khristiansen [15], many theoretical works and experimental measurements have been performed; however, the origin of this feature is still under debate. From the experimental point of view, measurements indicate that such a break is observed in the hadronic, muonic, and electromagnetic components (i.e. [16–24]), as well as in Cherenkov light (i.e. [25–28]). These results give a clear indication that the knee is a peculiarity of the primary spectrum, disfavoring a hypothesis based on changes of the interaction characteristics of the primaries with air nuclei. This conclusion has been reinforced by the first comparisons of the predictions from hadronic models and LHC data [29].

The experiments operate at different altitudes, ranging from ~4300 m of TIBET-ASγ to the sea level of KASCADE. In general, for experiments sampling EAS at the observation level, the height above sea level is crucial either for energy resolution and for sensitivity to composition. In general, near the shower's maximum, the number of particles is almost independent of the primary particle, and the fluctuations of EAS are minimized. Therefore, high altitudes are suitable for good energy resolution. On the other hand, experiments at sea level enhance the differences in the longitudinal development of EAS of different primaries, as the shower is sampled well after its maximum. Therefore, they are more suitable for composition studies; however, fluctuations are higher.

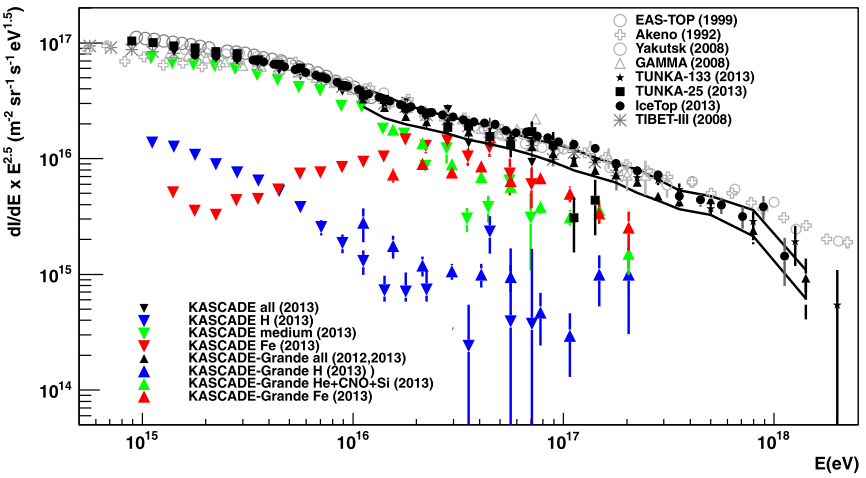

Fig. 1. (Color online.) All-particle energy spectrum as measured by [18,16,27,30,31,28,32–35] between 10^{15} and 10^{18} eV. The separation in mass groups obtained by KASCADE and KASCADE-Grande in [36] is shown as well. The two lines in the plot indicate the systematic uncertainty in the energy spectrum of KASCADE-Grande by interpreting the data using SIBYLL (top line) or EPOS (bottom line) interaction models. See text for details of this plot.

Fig. 1 shows the all-particle energy spectrum measured by several experiments. Despite the slight differences in flux, emphasized by multiplying the differential spectrum by $E^{2.5}$, the 'knee' is observed by all experiments around $\sim 4 \times 10^{15}$ eV. A general consensus does not exist yet on the chemical component mainly responsible for such a feature. Nevertheless, several experimental results associate it with the bending of the light component, and are compatible with a rigidity dependent cut-off [21,19,23,24]. Unfortunately, the flux of the different components vary significantly depending on the interaction model used to interpret the data [21]. However, if this interpretation is correct, the heavy component should show a similar bending in the energy range 5×10^{16}–10^{17} eV.

The first generation of arrays was mainly focused on the investigation of the knee region. They were characterized by a small spacing among detectors which limited the size of the array. Consequently, they tended to run out of statistics around 10^{17} eV, and were, therefore, unable to give a conclusive answer to the origin of the knee. In the last decade, a new generation of detectors was set up to study in detail the energy range between 10^{16} eV and 10^{18} eV, namely KASCADE-Grande [37], Tunka-133 [38] and IceTop [39] arrays. The present review focuses on the results obtained so far by these experiments.

The KASCADE-Grande experiment is an enlargement of the former KASCADE array obtained by using the plastic scintillation detectors formerly employed in the EAS–TOP experiment. The array operated from 2003 to 2012. For each event, the arrival direction, the number of charged particles (N_{ch}), and the number of muons (N_{μ}) at observation level are derived. These observables are used to estimate the primary energy on an event-by-event basis, and to classify events into samples generated by light and heavy primaries according to the ratio between the muon and charged particle numbers.

$$\log_{10}(E) = \left[a_{\mathrm{H}} + (a_{\mathrm{Fe}} - a_{\mathrm{H}}) \cdot k\right] \cdot \log_{10}(N_{\mathrm{ch}}) + b_{\mathrm{H}} + (b_{\mathrm{Fe}} - b_{\mathrm{H}}) \cdot k \tag{2}$$

$$k = \frac{\log_{10}(N_{\mathrm{ch}}/N_{\mu}) - \log_{10}(N_{\mathrm{ch}}/N_{\mu})_{\mathrm{H}}}{\log_{10}(N_{\mathrm{ch}}/N_{\mu})_{\mathrm{Fe}} - \log_{10}(N_{\mathrm{ch}}/N_{\mu})_{\mathrm{H}}} \tag{3}$$

$$\log_{10}(N_{\mathrm{ch}}/N_{\mu})_{\mathrm{H,Fe}} = c_{\mathrm{H,Fe}} \cdot \log_{10}(N_{\mathrm{ch}}) + d_{\mathrm{H,Fe}} \tag{4}$$

The parameters a, b, c, and d depend on the interaction model used to interpret the events. The k parameter is, by the definition of Eq. (3), a number centered around 0 for H-initiated showers and 1 for Fe ones if expressed as a function of N_{ch} for Monte-Carlo events. It is expected that the average values of the k parameter for the experimental events lie between the H and Fe limits. In case this is not verified, it would be a hint of some deficit of the model to describe the experimental events. Naturally, as the parameters a–d differ from model to model, the same experimental event might give distinct values of k when interpreted using various interaction models. The energy resolution varies between $\sim$30% at the energy threshold of 10^{16} eV and decreases below 20% at the highest energies (10^{18} eV).

Tunka-133 is an enlargement of the former Tunka-25 array. It is located at about 670 m above sea level in the Tunka Valley, Siberia. It consists of a compact array of 133 Cherenkov light detectors separated into 19 subarrays. The array was extended in 2011 by adding 6 more clusters around the previous array, at a distance of $\sim$1 km in order to enlarge the exposure for the events at highest energies. In each event the Amplitude Distance Function (ADF) is fitted. It was found that the Cherenkov light flux density at 200 m—$Q\,(200)$—is connected to the EAS energy E_0 by the relation:

$$E_0 = C \cdot Q\,(200)^g \tag{5}$$

with $g = 0.94$ obtained from CORSIKA simulation of an equal mixture of proton and iron primaries in the energy range 5×10^{15}–10^{18} eV. In order to reconstruct the EAS energy from Cherenkov light, in principle one has to know the absolute

sensitivity of Cherenkov detectors and the atmospheric transparency. To avoid these problems, in Tunka-133, the Cherenkov spectrum is normalized each night to a reference spectrum obtained via the QUEST experiment [40]. The energy resolution is of the order of 15%.

IceTop is the surface EAS array of the IceCube Neutrino Observatory at the Geographical South Pole. It is located on top of the Antarctic ice sheet at an altitude of ∼2850 m above sea level, which corresponds to an atmospheric depth of ∼700 g/cm^2, quite close to the proton shower maximum (550–750 g/cm^2 in the 10^{15}–10^{18}-eV energy range). In this way, the shower fluctuations are minimal and the energy resolution is 5%–10% in the entire energy range spanned by the experiment: 10^{15}–10^{18} eV. The IceTop array consists of 81 stations covering an area of ∼1 km^2, with an interstation separation of 125 m on average. Each station is formed by two ice Cherenkov tanks separated by 10 m. IceTop measures the EAS particle at the observation level, while IceCube can measure the muon bundles associated with the same EAS shower if the shower axis goes through the in-ice detector. This allows us to study also the chemical composition for coincidence events. Event by event, the energy is determined by measuring the lateral distribution function of the EAS. It is found from CORSIKA simulation that the energy depends on the particle density at 125 m from the core (S_{125}) by the following relation:

$$\log_{10}(E) = p_1 \log_{10}(S_{125}) + p_0 \tag{6}$$

The parameters p_1 and p_0 depend on the composition assumption, the zenith angle bin, and the spectral index.

The three experiments differ on the technique employed to derive the EAS characteristics, which imply also distinct capabilities and uncertainties in determining the energy spectrum and the mass composition. All three experiments give an energy based on the Monte-Carlo simulation results, which, however, do not have the same degree of uncertainty because different parameters are used for the energy assignment. KASCADE-Grande, by using the N_e–N_μ technique, is able to determine the energy spectrum without any a priori assumption on the primary composition. The separation between light and heavy primaries is emphasized by being located at sea level. However, the shower fluctuations, and the uncertainties in the description of the longitudinal development of the EAS in the atmosphere by means of hadronic interaction models, give a ±10% systematic effect in the absolute energy scale. The separation in heavy and light primaries is even much more uncertain in flux [35]. Anyway, the evolution of the flux of mass groups as a function of energy can be nicely determined.

In the case of Tunka, the expression (5) is essentially independent of the assumed composition and interaction model used in CORSIKA. The mass composition is determined through the depth of shower maximum ($X_{\max}$) and it is expressed only in terms of $\langle \ln(A) \rangle$. It is not possible to separate the events into mass groups [31].

IceTop uses the particle density at one given distance from the shower core, which is only slightly dependent on the interaction model (the flux varies by a few percents if SIBYLL [41] or QGSjet-II [42] are used to parameterize expression (6)). However, by measuring only the shower's size, the detector is insensitive to composition. Hence, to determine the energy spectrum, an a priori assumption on composition is needed. A difference in flux of the order of a factor of 2 below 10^{16} eV is derived assuming a pure proton or iron composition (see [32]). The IceTop spectrum published in [32] assumes a mixed composition called H4a, which is described by Gaisser in [43]. Keeping in mind the differences among the techniques, a comparison of the results of these three experiments allows understanding possible systematic uncertainties of each method, and cross-checking common features in the spectrum.

Fig. 1 reports the energy spectrum as published by the three experiments in [34,31,32]. The KASCADE-Grande spectrum is based on QGSjet-II interaction model and depends on the composition determined on an event-by-event basis using the N_{ch}–N_μ ratio (k parameter of Eq. (3)). Two lines are also drawn, which represent the flux obtained using SIBYLL (top line) or EPOS1.99 [44] (bottom line) models to interpret the experimental events. IceTop spectrum is based on SIBYLL parameterization with the composition from the H4a model. Tunka-133 simulations are based on CORSIKA QGSjet-II.

The difference in flux between the three experiments would vanish by applying a ∼5% energy shift down to IceTop events and ∼5% up to KASCADE-Grande ones, which are well inside the systematic uncertainties of the two experiments. The apparent larger difference in the results is due to the way of plotting the differential spectrum multiplied by $E^{2.5}$. Part of the systematic uncertainty has to be ascribed to the interaction model employed to assign the energy. If SIBYLL is adopted for KASCADE-Grande events as in IceTop, the two spectra are in much better agreement (see top line in Fig. 1). This is expected for KASCADE-Grande, as there is a ∼10% shift between the energy assignment of events using QGSjet-II or SIBYLL models [35]. Nevertheless, this is not the only source of difference in the results. The energy spectrum of IceTop is obtained adopting the H4a model, which gives a flux similar to that observed with a pure He composition [32]. However, the average mass composition of KASCADE-Grande using SIBYLL or QGSJet-II interaction is heavier (between CNO and Si). Therefore, if the same composition model would be applied to both experiments, the two spectra will be slightly shifted apart, even though, still inside the systematic uncertainties of the experiments.

Keeping in mind the above discussion, Fig. 1 shows that for all three experiments, the all-particle energy spectrum in the range 10^{16}–10^{18} eV cannot be fitted by a single power law. The spectrum shows a spectral hardening at $\sim 2 \times 10^{16}$ eV and a steepening at $\sim 10^{17}$ eV. This result was first pointed out by KASCADE-Grande in [45] and then more firmly assessed by successive analyses [34,35]. Recently, it has been confirmed with higher statistics and precision by Tunka-133 and IceTop-73 [31,32], in particular for the feature at $\sim 2 \times 10^{16}$ eV.

Table 1 shows a summary of the spectral indexes obtained by the three experiments in this energy range. Every experiment indicates a slope $\gamma > 3.1$ between $15.8 < \log_{10}(E/\text{eV}) < 16.3$. The spectrum gets harder in the energy range $16.3 < \log_{10}(E/\text{eV}) < 17.0$, where $\gamma < 3.0$ and then gets softer again above $\log_{10}(E/\text{eV}) > 17.0$ with $\gamma > 3.2$. While

Table 1
Slopes of the energy spectrum in different energy ranges as obtained by IceTop, Tunka and KASCADE-Grande. The uncertainties in the slopes include statistical and systematic ones.

Experiment	$\log_{10}(E/\text{eV})$	γ	$\log_{10}(E/\text{eV})$	γ	$\log_{10}(E/\text{eV})$	γ
IceTop	15.80–16.20	3.14 ± 0.03	16.30–17.00	2.90 ± 0.04	17.15–17.90	3.37 ± 0.15
Tunka-133	15.80–16.30	3.23 ± 0.06	16.30–17.50	3.00 ± 0.06	17.50–18.00	3.33 ± 0.20
KASCADE-Grande	16.00–16.30	>3.10	16.30–16.90	2.95 ± 0.05	17.00–18.00	3.24 ± 0.08

the position of the last break of Tunka-133 spectrum is compatible with the so-called 'second knee' [46,16], IceTop and KASCADE-Grande indicate a break at lower energies. None of the experiments supports the 'bump' at $6\text{–}8 \times 10^{16}$ eV claimed by GAMMA [30].

3. The composition

Below 10^{18} eV, the two most common techniques to infer the chemical composition are the measurement of the shower and muon sizes (N_{ch}–N_{μ}), and the detection of the Cherenkov light. In both methods, a comparison with EAS simulations is needed to interpret the data in terms of primary mass. In case of N_{ch}–N_{μ}, the number of charged particles is related to the primary energy, while the ratio $N_{\text{ch}}(N_{\text{e}})/N_{\mu}$ is an estimator of the primary mass. In case of Cherenkov light detection, primary energy and mass are derived from the shape of the ADF. The ADF is characterized by a prominent shoulder at around 120 m. The slope of the ADF measured within 120 m is found to depend on the height of the shower's maximum and hence on the mass of the primary particle. On the other hand, the overall Cherenkov intensity at distances above the shoulder provides a calorimetric measurement of the energy.

KASCADE-Grande and IceTop (in coincidence with IceCube) exploit the N_{ch}–N_{μ} technique, while Tunka-133 the Cherenkov light method. It is interesting to compare the results as they complement each others. While KASCADE-Grande uses the low-energy muons ($E_{\mu} > 230$ MeV), IceTop relies on the high-energy muon bundles detected by IceCube ($E_{\mu} > 500$ GeV). The peculiarity of measuring TeV muons is that they probe the energy per nucleon, while the low-energy particles at surface array investigate the energy per particle. The disadvantage is that the solid angle is small, which limits the overall statistics that can be collected. This technique was already applied in the past by EAS–TOP and MACRO (from $\sim 10^{13}$ eV till above 10^{16} eV [11,20]) and at the Baksan underground laboratory [47]. By means of the N_{ch}–N_{μ} method, a separation into mass groups, or at least into heavy and light groups, is feasible and this leads to the determination of the spectra of mass groups. The level at which the separation is possible depends on the resolution of the detector and on the refinement of the algorithms employed to analyze the events. In fact, EAS fluctuations in the shower's development are very important, and electron and muon sizes are not independent. However, a two-dimensional unfolding can properly take into account such fluctuations as originally employed by KASCADE [21]. On the other hand, the Cherenkov technique so far allowed determining only the average logarithmic mass of CR as a function of energy.

In KASCADE-Grande, different methods have been adopted to derive the composition. The first two are based on the ratio N_{μ}/N_{ch}. The main aim is the separation of the events into heavy and light mass groups. No correction for shower fluctuations is applied. The first one relies on the parameter k in Eq. (3), which is determined by taking into account the calibration functions in Eq. (4) defined for each zenith angular bin. The results of the different bins are summed up at the very end. Each event is classified heavy or light, depending on whether the k value is higher or lower than a threshold value ($k_{\text{thr}}(E)$) variable with energy. The second method uses the parameter Y defined as: $Y = \frac{\log_{10} N_{\mu}(\theta_{\text{ref}})}{\log_{10} N_{\text{ch}}(\theta_{\text{ref}})}$, which takes into account the shower attenuation in atmosphere by converting the shower size and the muon number measured at a zenith angle θ, by means of the Constant Intensity Cut technique, to the reference angle $\theta_{\text{ref}} = 22°$ [48]. Also in this case, each event is classified heavy or light depending on whether the Y value is higher or lower than a threshold value (Y_{thr}), which is constant with energy. Unlike k, Y is a pure experimental value. Only Y_{thr} is defined as a function of the interaction model used to interpret the events. The energy is assigned event-by-event for both methods using Eq. (2). The main results of these analyses have been reported in [49,50] using QGSjet-II. A knee is observed in the heavy component of CR at $E = 10^{16.92 \pm 0.04}$ eV, which coincides inside the uncertainties with the change of slope in the all-particle energy spectrum around 10^{17} eV (see Table 1). The spectral index changes from $\gamma_1 = -2.76 \pm 0.02$ below the knee to $\gamma_2 - 3.24 \pm 0.05$ above it. At slightly higher energies ($E = 10^{17.08 \pm 0.09}$ eV), the light component shows a hardening of the slope, with the spectral index changing from $\gamma_1 = -3.25 \pm 0.06$ below this ankle-like structure to $\gamma_2 - 2.79 \pm 0.09$ above it. These findings obtained with QGSjet-II are confirmed by successive analyses using other interaction models (EPOS, SIBYLL), as shown in [35,48]. Naturally, the positions of the changes of slope as well as the intensities of the different components depend on the interaction model adopted to interpret the experimental events. The knee in the heavy component is visible also in the all-particle spectrum, as it is the dominant component.

In the third approach, the composition is extracted using the same unfolding technique previously employed on KASCADE events [36]. This technique is applied only to the most vertical showers ($\theta < 18°$), which reduces the covered energy range compared to the other methods. However, it allows separating the data in five different mass groups. As shown in [36], the results of KASCADE-Grande are in nice agreement with those of KASCADE in the overlapping energy range, and they confirm the findings on the knee of the heavy component at $\sim 8 \times 10^{16}$ eV, as well as the shape and intensity of the all-particle

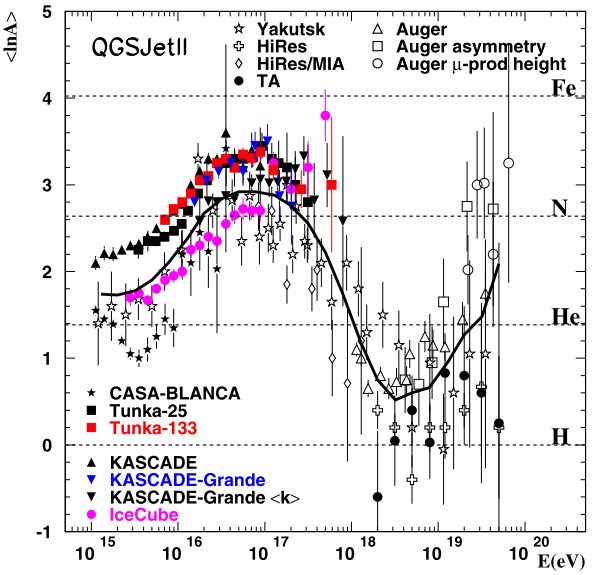

Fig. 2. (Color online.) Average logarithmic mass of CR as a function of energy derived from $X_{\max}$ and particle detector measurements using QGSJet-II interaction model. Most of the data are taken from [52] and references therein. The others are from [31,51,36,49]. The solid line is drawn as a guidance and is obtained by averaging, in each energy bin, the values of $\langle \ln A \rangle$ reported in the figure.

energy spectrum. Moreover, the knee is clearly associated with the bending of the iron component. In the last energy bins, a slight indication of the recovery of the light component as found in [50] is visible, although not statistically significant. The spectral steepening of the heavy component occurs at an energy where the charge-dependent knee of iron is expected, if the knee at about $3–5 \times 10^{15}$ eV is assumed to be caused by a decrease in flux of light primaries (proton and/or helium).

The Tunka-133 experiment derived the mass composition by using the $X_{\max}$ measurement and interpreting the events using the QGSjet-II-04 interaction model, which is the revised version of the model after LHC data. The points in Fig. 2 are rescaled to QGSjet-II-03 to be comparable with the other experiments. Two methods of $X_{\max}$ reconstruction were developed [31]: the first is based on the shape of the ADF, while the second on the width of the Cherenkov pulses. From the $\langle X_{\max} \rangle$ vs. primary energy dependence, the mean values of $\langle \ln A \rangle$ is extracted by interpolation. The results indicate that the mass composition becomes heavier in the energy range $10^{16}–3 \times 10^{16}$ eV, then stays heavy till 10^{17} eV, where the composition starts becoming lighter. These results are quantitatively in agreement with KASCADE-Grande findings.

Preliminary results on the mass composition on coincident events between IceTop and IceCube have been reported in [51]. They are based on one year of data taking between 2010 and 2011 using IceCube-79 and IceTop-73 with a zenith angle $\theta < 37°$. The muon multiplicity is the composition-dependent parameter. Experimental data were compared with expectations from simulations (SIBYLL and QGSjet-II interaction models). A neural network was trained with Monte-Carlo simulations of four primaries (proton, helium, oxygen, and iron) to solve the non-linear mapping of primary energy, mass, and reconstructed variables. The results indicate an increase of $\langle \ln A \rangle$ in the energy range $10^{16}–3 \times 10^{17}$ eV.

Fig. 2 compares the results of several experiments in terms of $\langle \ln A \rangle$, as it is often reported in the literature to describe the evolution of the composition as a function of energy. Only QGSJet-II model is considered. A more detailed description including the role of interaction models in composition is reported in [52], where most of the data are taken from. Use of different models introduces a shift in the average mass comparable to the dispersion of the data in Fig. 2. Despite the large uncertainty in the absolute composition, a common general trend is visible. Composition gets heavier through the knee region and becomes lighter approaching the ankle. The solid line in the plot is used as a guidance line to show how the average $\langle \ln A \rangle$ from the data in the plot evolves with energy.

4. Anisotropy

The search for anisotropies in the arrival direction of CR around the knee region can provide relevant information to distinguish source and propagation effects. A lot of progress has been made in the past years in the TeV energy range and at higher energies by several experiments in the study of small- and large-scale anisotropies [53–57]. Large-scale anisotropies of the order of $10^{-3}–10^{-4}$ have been detected. The anisotropy varies with energy, but the topological structure remains the same till around 10^{14} eV, where an abrupt change occurs, as pointed out by IceCube and IceTop [58]. Such a change is confirmed till knee energies ($\sim 2 \times 10^{15}$ eV). This result seems to be inconsistent with the amplitude and phase expected according to the Compton-Getting prediction due to the relative motion of the Earth in the Galaxy [59]. A detailed review of the possible explanations of the observed topology can be found in [58]. KASCADE-Grande published recently [60] an update on the anisotropy study based on the East–West method [61]. The analysis has been performed on the entire data

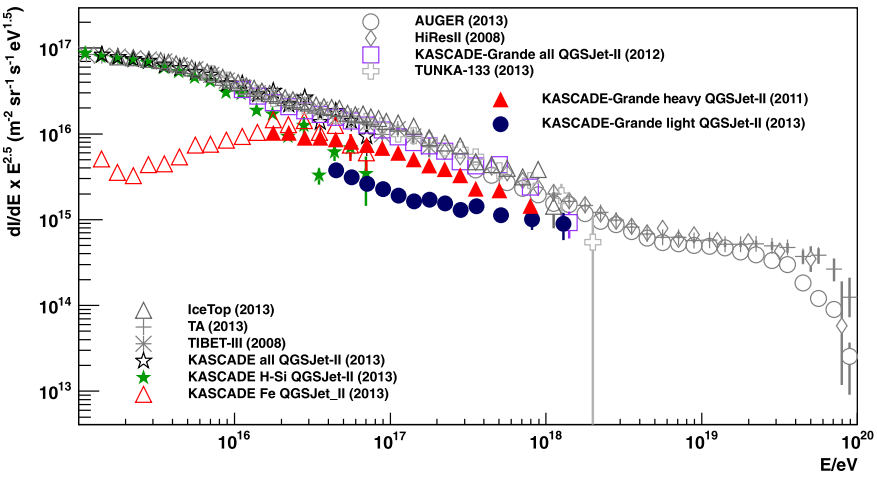

Fig. 3. (Color online.) The measurement of the CR spectrum by EAS experiments from the knee till the end of the spectrum. The main knee is explained as the bending of the light, followed by the medium components. The fainter knee around 10^{17} eV is attributed to the bending of the heavy one. An ankle-like feature is observed in the light component just above 10^{17} eV, which might be related to the lightening of the composition approaching the ankle.

set ($\theta < 40^\circ$ and $E > 2.6 \times 10^{15}$ eV). An upper limit on the amplitude of 0.47×10^{-2} at the 99% c.l. was derived. By investigating the variation of the amplitude as a function of energy, it was found that the amplitudes were not significant, however, the phases were in almost all energy bins centered around 250 ± 25 degrees. This is interesting in itself because it points towards the Galactic Center. Moreover, it agrees inside the statistical uncertainties with the results of the anisotropy studies of the Pierre Auger Observatory [62] in the energy range 3×10^{17}–10^{18} eV.

5. Approaching the ankle

The energy range between 10^{17} eV and 10^{19} eV is considered the region where a transition between Galactic and extragalactic radiation occurs. The location and the composition at the turn energy is highly dependent on the theoretical model. In case of the dip model [6], the transition from heavy Galactic nuclei to extragalactic proton and helium has to take place below 10^{18} eV. Therefore, already below it, the light component should be the dominant one. Quite different is the case of the classical ankle model [63], where the transition occurs around the ankle ($\sim 5 \times 10^{18}$ eV). Therefore, the Galactic component of CR is significant till these energies. Finally, in case of the mixed-composition model [64] the extragalactic CR are accelerated with a chemical composition similar to the GeV Galactic one. Their composition changes in propagation because of photoproduction, electron positron pair creation, and nuclear photodisintegration. The transition between Galactic and extragalactic CR occurs at intermediate energies compared to those in the other two models, and the energy spectrum and composition strongly depend on the distance of the extragalactic sources.

In order to discriminate which model explains correctly the experimental data, a sufficiently high statistics is needed in the energy range 10^{17}–10^{19} eV. Unfortunately, around 5×10^{17}–2×10^{18} eV, the experiments at the knee (KASCADE-Grande, Tunka-133 and IceTop) start running out of statistics, while in the original design, Auger [65] and Telescope Array (TA) [66] were planned to work at higher energies. In the recent years, an effort has started to lower the energy threshold of Auger and TA by adding further components. TA is planning to add high elevation fluorescence telescopes and new scintillator counters with a finer spacing (TALE) to reach a threshold around $10^{16.5}$ eV. At Auger site, the High Elevation Auger Telescope (HEAT [67]) and the Auger Muon and Infill for the Ground Array recently installed (AMIGA [68]) allowed decreasing the energy threshold of Auger to 3×10^{17} eV. The latest results of the energy spectrum of Auger [69], which include also such contributions, are presented in Fig. 3. It is interesting to observe that, after the re-calibration of the energy scale of Auger, there is a good matching between the fluxes measured by KASCADE-Grande, Tunka-133 and IceTop-73 at low energies with those obtained by Auger and TA at higher energies in the overlapping range. Indeed the systematic differences on flux between KASCADE-Grande and IceTop are of the same order as between Auger and TA. This is not obvious per se as the low-energy experiments rely on the energy assignment by means of hadronic interaction models, while the giant detector arrays are calibrated by means of the fluorescence light detected in coincidence events. Being bracketed by, and in fair agreement with, the direct measurements at low energies and the fluorescence method at the highest ones, the experiments at the knee provide a quite reliable picture of the energy shape and intensity in the energy range between 10^{15} eV and 10^{18} eV.

HiRes, HiRes/MIA and Yakutsk results show that the composition becomes lighter between 10^{17} eV and 10^{18} eV. The $\langle \ln A \rangle$ inferred by Auger and TA at the threshold is compatible with proton composition. In the forthcoming years, it is desirable to be able to separate the events into mass groups as performed at the knee energies. This will help understanding which theoretical model properly describes the transition between Galactic and extragalactic CR. This is one of the main motivation of the AMIGA upgrade at Auger. In parallel, measurements at LHC will contribute to the fine tuning of the

hadronic interaction models, which are one of the main sources of uncertainty on the absolute flux of the different mass groups.

The anisotropy study performed by Auger indicate no significant anisotropy at energies above 10^{18} eV. The phase of the anisotropy seems to be consistent with KASCADE-Grande findings below 10^{18} eV, while it turns at higher energies. The origin of this phase-turn is another question that needs to be addressed in the future.

6. Conclusions

A lot of progress has been made in the past 50 years since the discovery of the knee. In the current understanding, the features seen in the energy spectrum between 10^{15} eV and 10^{18} eV are compatible with the bending of the different components of CR, supporting a rigidity dependence of the phenomena. Whether this is related to Galactic diffusion or limitations of the accelerators is still unclear, as the anisotropy studies do not allow one to settle the question yet. Approaching the ankle, the composition gets lighter, and there are hints that the light component has a harder spectrum; however, it needs confirmation. Therefore, in the next decade the attention should focus on the energy range between 10^{17} eV and 10^{19} eV to clarify the origin of the ankle that still remains unsettled. The low energy upgrade plans of Auger and TA are expected to properly address this question.

References

[1] A. Giuliani, et al., AGILE Collaboration, Astrophys. J. 742 (2011) L30.
[2] M. Ackermann, et al., FERMI-LAT Collaboration, Science 339 (2013) 807.
[3] A.M. Hillas, J. Phys. G, Nucl. Part. Phys. 31 (2005) R95.
[4] T.K. Gaisser, T. Stanev, S. Tilav, arXiv:1303.3365v1, 2013.
[5] B. Peters, Il Nuovo Cimento 22 (1961) 800.
[6] V. Berezinsky, A. Gazizov, S. Grigorieva, Phys. Rev. D 74 (2006) 043005.
[7] A. Castellina, F. Donato, in: Planets, Stars and Stellar Systems, vol. 5, 2012.
[8] M. Bertaina, J. Phys. Soc. Jpn. Suppl. A 78 (2009) 210.
[9] T. Antoni, et al., KASCADE Collaboration, Astrophys. J. 602 (2004) 914.
[10] M. Aglietta, et al., EAS-TOP Collaboration, Astropart. Phys. 19 (2003) 329.
[11] M. Aglietta, et al., EAS-TOP Collaboration, Astropart. Phys. 21 (2004) 223.
[12] B. Bartoli, et al., ARGO Collaboration, Phys. Rev. D 85 (2012) 092005.
[13] Y.S. Yoon, et al., CREAM Collaboration, Astrophys. J. 728 (2011) 122.
[14] D. Heck, et al., Report FZKA 6019, 1998.
[15] G.V. Kulikov, G.B. Khristiansen, J. Exp. Theor. Phys. 35 (1958) 635.
[16] M. Nagano, et al., AKENO Collaboration, J. Phys. G 18 (1992) 423.
[17] M.A.K. Glasmacher, et al., CASA-MIA Collaboration, Astropart. Phys. 10 (1999) 291.
[18] M. Aglietta, et al., EAS-TOP Collaboration, Astropart. Phys. 10 (1999) 1.
[19] M. Aglietta, et al., EAS-TOP Collaboration, Astropart. Phys. 21 (2004) 583.
[20] M. Aglietta, et al., EAS-TOP Collaboration, Astropart. Phys. 20 (2004) 641.
[21] T. Antoni, et al., KASCADE Collaboration, Astropart. Phys. 24 (2005) 1.
[22] M. Amenomori, et al., TIBET-Asγ Collaboration, Phys. Lett. B 632 (2006) 58.
[23] A.P. Garyaka, et al., GAMMA Collaboration, Astropart. Phys. 28 (2007) 169.
[24] H. Tanaka, et al., GRAPES Collaboration, J. Phys. G, Nucl. Part. Phys. 39 (2012) 025201.
[25] J.W. Fowler, et al., CASA-BLANCA Collaboration, Astropart. Phys. 15 (2001) 49.
[26] F. Arqueros, et al., HEGRA Collaboration, Astron. Astrophys. 359 (2000) 682.
[27] A.A. Ivanov, S.P. Knurenko, I.Y. Sleptsov, Yakutsk Collaboration, New J. Phys. 11 (2009) 065008.
[28] N. Budnev, et al., TUNKA-25 Collaboration, Astropart. Phys. 50–52 (2013) 18.
[29] S. Ostapchenko, Prog. Theor. Phys. Suppl. 193 (2012) 204.
[30] A.P. Garyaka, et al., GAMMA Collaboration, J. Phys. G, Nucl. Part. Phys. 11 (2008) 115201.
[31] V.V. Prosin, et al., TUNKA-133 Collaboration, in: 33rd ICRC, 2013, p. #0617.
[32] M.G. Aartsen, et al., ICE-TOP Collaboration, Phys. Rev. D 88 (2013) 042004.
[33] M. Amenomori, et al., TIBET-Asγ Collaboration, Astrophys. J. 678 (2008) 1165.
[34] W.D. Apel, et al., KASCADE-Grande Collaboration, Astropart. Phys. 36 (2012) 183.
[35] W.D. Apel, KASCADE-Grande Collaboration, Adv. Space Res. (2013), http://dx.doi.org/10.1016/j.asr.2013.05.008.
[36] W.D. Apel, et al., KASCADE-Grande Collaboration, Astropart. Phys. 47 (2013) 54.
[37] W.D. Apel, et al., KASCADE-Grande Collaboration, Nucl. Instrum. Methods A 620 (2010) 202.
[38] S.F. Berezhnev, et al., Tunka-133 Collaboration, Nucl. Instrum. Methods A 692 (2012) 98.
[39] R. Abbasi, et al., IceTop Collaboration, Nucl. Instrum. Methods A 700 (2013) 188.
[40] E.E. Korolsteva, et al., QUEST Collaboration, Nucl. Phys. B, Proc. Suppl. 165 (2007) 74.
[41] J. Engel, et al., Phys. Rev. D 46 (1992) 5013.
[42] S. Ostapchenko, et al., Phys. Rev. D 74 (2006) 014026/1.
[43] T. Gaisser, Astropart. Phys. 35 (2012) 801.
[44] K. Werner, et al., Phys. Rev. C 74 (2006) 044902/1.
[45] M. Bertaina, et al., KASCADE-Grande Collaboration, Astrophys. Space Sci. Trans. 7 (2011) 229.
[46] D.R. Bergman, J.W. Belz, J. Phys. G 34 (2007) R359.
[47] V. Bakatanov, et al., BAKSAN Collaboration, Astropart. Phys. 12 (1999) 19.
[48] A. Chiavassa, et al., KASCADE-Grande Collaboration, in: 33rd ICRC, 2013, p. #0092.
[49] W.D. Apel, et al., KASCADE-Grande Collaboration, Phys. Rev. Lett. 107 (2011) 171104.
[50] W.D. Apel, et al., KASCADE-Grande Collaboration, Phys. Rev. D 87 (2013) 081101(R).
[51] A. Tamburro, et al., IceCube Collaboration, arXiv:1307.8394v1, 2013.

[52] K.-H. Kampert, M. Unger, Astropart. Phys. 35 (2012) 660.
[53] R. Iuppa, et al., ARGO Collaboration, J. Phys. Conf. Ser. 409 (2013) 012039.
[54] A. Abdo, et al., MILAGRO Collaboration, Phys. Rev. Lett. 101 (2008) 221101.
[55] M. Aglietta, et al., EAS-TOP Collaboration, Astrophys. J. Lett. 692 (2009) L130.
[56] R. Abbasi, et al., IceCube Collaboration, Astrophys. J. Lett. 718 (2010) L194.
[57] M. Amenomori, et al., TIBET-ASγ Collaboration, Science 314 (2006) 439.
[58] P. Desiati, et al., IceCube Collaboration, arXiv:1308.0246v1, 2013.
[59] A.H. Compton, I.A. Getting, Phys. Rev. 47 (1935) 817.
[60] A. Chiavassa, et al., KASCADE-Grande Collaboration, in: 33rd ICRC, 2013, p. #0093.
[61] R. Bonino, et al., Astrophys. J. 738 (2011) 67.
[62] P. Abreu, et al., Auger Collaboration, Astropart. Phys. 34 (2011) 627.
[63] E. Waxman, Astrophys. J. 452 (1995) L1.
[64] D. Allard, Astropart. Phys. 39–40 (2012) 33.
[65] J. Abraham, et al., Auger Collaboration, Nucl. Instrum. Methods 523 (2004) 50.
[66] T. Abu-Zayyad, et al., TA Collaboration, Nucl. Instrum. Methods A 689 (2012) 87.
[67] T.H.-J. Mathes, et al., Auger Collaboration, in: 32nd ICRC, 2011, p. #0761.
[68] F. Sanchez, et al., Auger Collaboration, in: 32nd ICRC, 2011, p. #0742.
[69] A. Aab, et al., Auger Collaboration, arXiv:1307.5059v1, 2013.